Full-Scale Bridge Finite-Element Model Calibration Using Measured Frequency-Response Functions

Jesse D. Sipple, M.ASCE[1]; and Masoud Sanayei, M.ASCE[2]

Abstract: A frequency-response function–based parameter-estimation method was used for finite-element (FE) model calibration of a full-scale bridge using measured dynamic test data. Dynamic tests were performed on the bridge to obtain measured frequency-response functions. Data quality was ensured by comparing measured data with the FE model and removing erroneous data. A coherence data selector was developed to remove the noise-contaminated portions of the measured frequency-response functions. An unrefined FE model was created using design information for the geometry and structural parameters. This model was improved to a refined model by using concrete cylinder property data, as-built drawing geometry, and the addition of components that participate in the dynamic response of the bridge. Simulations were performed using the model to ensure both observability and identifiability of structural parameters. The model of the bridge was then calibrated successfully using measured frequency-response functions. An increase in the negative bending region concrete-deck rigidity was found during the calibration and verified by increased reinforcement in that area. Examining the second norm of the residual between the different models and the measured data resulted in an improvement from the unrefined to the calibrated FE model. The proposed method proved to be robust in the presence of modeling and measurement errors and computationally efficient for use with full-scale structures. **DOI: 10.1061/(ASCE)BE.1943-5592.0000705.**

Author keywords: Frequency-response function; Parameter estimation of structures; Finite-element (FE) model calibration; Optimization; Full-scale bridge; Dynamic testing.

Introduction

One of the tools available to bridge owners for bridge management is the practice of structural health monitoring (SHM). The field of SHM covers a vast range of different research topics from non-destructive evaluation techniques to output-only non-physics-based modeling. Further insight into the field of SHM can be found in Farrar and Worden (2007), Mottershead and Friswell (1993), Sohn et al. (2004), Ettouney and Alampalli (2011), and Karbhari and Ansari (2009). This paper focuses on solving the inverse problem for parameter estimation of physics-based finite-element (FE) models. The ASCE Structural Engineering Institute Committee on Structural Identification of Constructed Systems recently released a report (Catbas et al. 2013) that covers many of the specific details of parameter estimation. This paper presents the application of a frequency-response function (FRF)–based FE model updating technique applied to a full-scale bridge.

These FRFs have been used in the literature with full-scale bridges. In Farrar and Jauregui (1998), FRFs were measured during the I-40 test, where the bridge was physically damaged using torches. Although FRFs were measured, the FRFs themselves were not used, and instead, natural frequencies, mode shapes, and damping ratios were extracted. Structural testing on the Millennium Bridge in London, England, was performed by Pavic et al. (2002) to detect vertical and lateral modes for remediation of vibration issues. Again, FRFs were obtained, and natural frequencies, mode shapes, and damping ratios were extracted. Vibration testing on a footbridge was performed by Živanović et al. (2007) to verify and calibrate design models, and again, FRFs were obtained, but only to extract natural frequencies and mode shapes. A full explanation of FRFs and current methods can be found in Ewins (2000).

The predominant cases in the literature show how FRFs can be used in FE model updating for either simulated or small laboratory structures. The publications that measure FRFs on full-scale bridges only use the FRFs to extract modal information, as shown in the three publications listed earlier. No publications have been found by the authors that perform FE model updating directly on a full-scale bridge using measured FRFs.

In this paper, a FE model updating method is applied to a full-scale bridge using measured FRFs. Parameter estimation is performed using both simulations and measured data for FE model calibration. Whereas natural frequencies and mode shapes provide discrete dynamic characteristics over a given frequency range, FRFs provide continuous dynamic characteristics over that same range, resulting in more information. This unique characterization leads to FRFs being referred to as a bridge signature. Techniques are presented that show how to accurately model a structure to simulate dynamic behavior. Additional studies were performed to examine observability and identifiability to ensure the accuracy of estimated parameters during model calibration. Additional details from this research can be found in Sipple (2014).

Powder Mill Bridge

The Powder Mill Bridge (PMB), which carries Vernon Avenue over the Ware River in Barre, Massachusetts, was commissioned in

[1]Testing and Analysis Structural Engineer, Bridge Diagnostics, Inc., 1995 57th Court North, Ste. 100, Boulder, CO 80301; formerly, Ph.D. Candidate, Dept. of Civil and Environmental Engineering, Tufts Univ., Medford, MA 02155. E-mail: jesses@bridgetest.com

[2]Professor, Dept. of Civil and Environmental Engineering, Tufts Univ., Medford, MA 02155 (corresponding author). E-mail: masoud.sanayei@tufts.edu

Note. This manuscript was submitted on March 21, 2014; approved on September 10, 2014; published online on October 6, 2014. Discussion period open until March 6, 2015; separate discussions must be submitted for individual papers. This paper is part of the ***Journal of Bridge Engineering***, © ASCE, ISSN 1084-0702/04014103(11)/$25.00.

September 2009 and is shown in Fig. 1. The bridge is 47 m long with two 11.75-m end spans and a 23.5-m midspan. The 200-mm steel-RC deck acts compositely, via shear studs, with six steel girders for the first two spans, and two more girders are added for the widened third span. The roadway has a travel width of 10 m, with a 1.8-m sidewalk on one side, and carries two lanes of traffic. Steel-reinforced elastomeric bearing pads support the steel girders at each pier and abutment. The PMB was instrumented with over 200 sensors during its construction, making the PMB one of the most instrumented bridges of its size and allowing the bridge to function as a full-scale outdoor research laboratory. The sensors were installed for both long-term monitoring and to capture data from periodic load tests. Three diagnostic truck-load tests were performed in 2009, 2010, and 2011. In addition to the truck tests, dynamic testing also was performed in 2010 and 2011. Use of measured static data from these tests is described in Sanayei et al. (2012) and Bell et al. (2013).

Dynamic Testing

The 2010 and 2011 dynamic bridge tests on the PMB used an APS Dynamics 400 Series shaker (APS Dynamics, San Juan Capistrano, California) with a moving mass of 30.6 kg to excite the bridge. Wilcoxon 731A accelerometers and P31 signal conditioners (Wilcoxon Research, Gaithersburg, Maryland) were used to measure the response of the bridge. A Wilcoxon 799M with P31 signal conditioner was used to measure the input excitation. The typical shaker and accelerometer setup is shown in Fig. 2. The instrumentation and testing techniques used were the outcome of a feasibility test performed on the bridge. This feasibility test allowed different excitation techniques and sensor types to be tested prior to mobilization. Results from this feasibility test showed that a hand-held instrumented sledge hammer did not provide adequate excitation compared with the shaker.

The portable shaker was moved to nine separate locations on the bridge deck for both the 2010 and 2011 tests, as shown in Fig. 3. The responses were measured at all nine locations per test, resulting in a total of 81 measured FRFs. The locations for sensor placement were determined based on the number of available sensors and arranged in a grid pattern to capture bending and torsional responses. The magnitude of the shaker excitation was approximately 45 N, corresponding to an acceleration level of 0.15g. The resulting response was measured between 1 and 6 mg.

The 2010 test used a linear sine sweep from 3 to 30 Hz as the input signal into the shaker. Each signal was repeated five times per location to obtain good-quality FRFs with high coherences. The duration and number of times the signal was repeated were determined during the feasibility test. The use of two or three signal repeats led to FRFs that were not as clean as when five or more repeats were used. Additional constraints, such as time limitations for the closure of the bridge, were also considered.

The 2011 dynamic load test used stepped sine sweeps from 2 to 40 Hz with a 0.5-Hz step increment. The change from linear sine sweep to stepped sine sweep was made to determine which signal would excite the bridge more efficiently, thus creating better FRFs. The length of each increment was the greater of 5 s or 100 cycles. Three ambient vibration readings were also taken throughout the test day. The purpose of these measurements was to determine whether the noise level changed, and analysis of the data showed that the noise level remained the same. The excitation and response signals were supplied and measured at a sampling rate of 2,000 Hz for both the 2010 and 2011 tests. The sample FRF shown for simulations and calibration in this paper is for the response at Node 7 as a result of excitation at Node 11, denoted by $\overline{H}_{7,11}$. This sample FRF is similar to the other FRF pairs that are not shown and represents a typical comparison between analytical and either measured or simulated data.

Fig. 1. PMB over the Ware River in Barre, Massachusetts (images by Jesse D. Sipple)

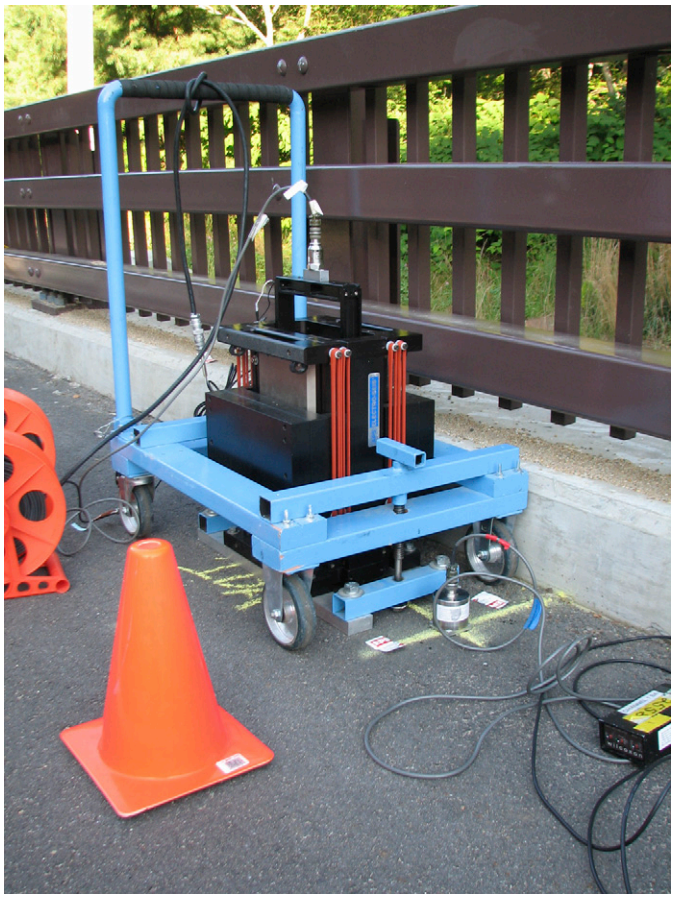

Fig. 2. Shaker and accelerometer setup for dynamic load testing (image by Jesse D. Sipple)

Data Quality

The presence of measurement noise must be carefully considered because it can contaminate parameter estimates.

Coherence Data Selector

A data selector was developed to remove noisy data using each sensor's measured coherence. A sample of the coherence data selector is shown in Fig. 4. The data not used, with poor coherence, are shown in the FRF plot. Studies were performed in which the measured noise from the PMB tests was added to the simulated response, coherences and FRFs were calculated, different cutoff values were selected, and parameter estimation was performed knowing the true expected parameter values. The coherence cutoff level of 0.90, shown as a horizontal line in the Fig. 4 coherence plot, offered a fine balance between computation time and accuracy of the unknown parameters. All the data presented in this paper were filtered using the coherence selector with a cutoff value of 0.90. The major advantage of the coherence data selector is that within a given FRF, only the noisy portions of the data are removed, allowing for the remainder of the data to be used in parameter estimation.

Usability of Measured FRFs

The measured data from the 2011 dynamic test were also compared with the refined model. This comparison was done to ensure that the general shape of the FRFs was correct. This comparison verified that the shaker and sensors were not placed at incorrect locations during

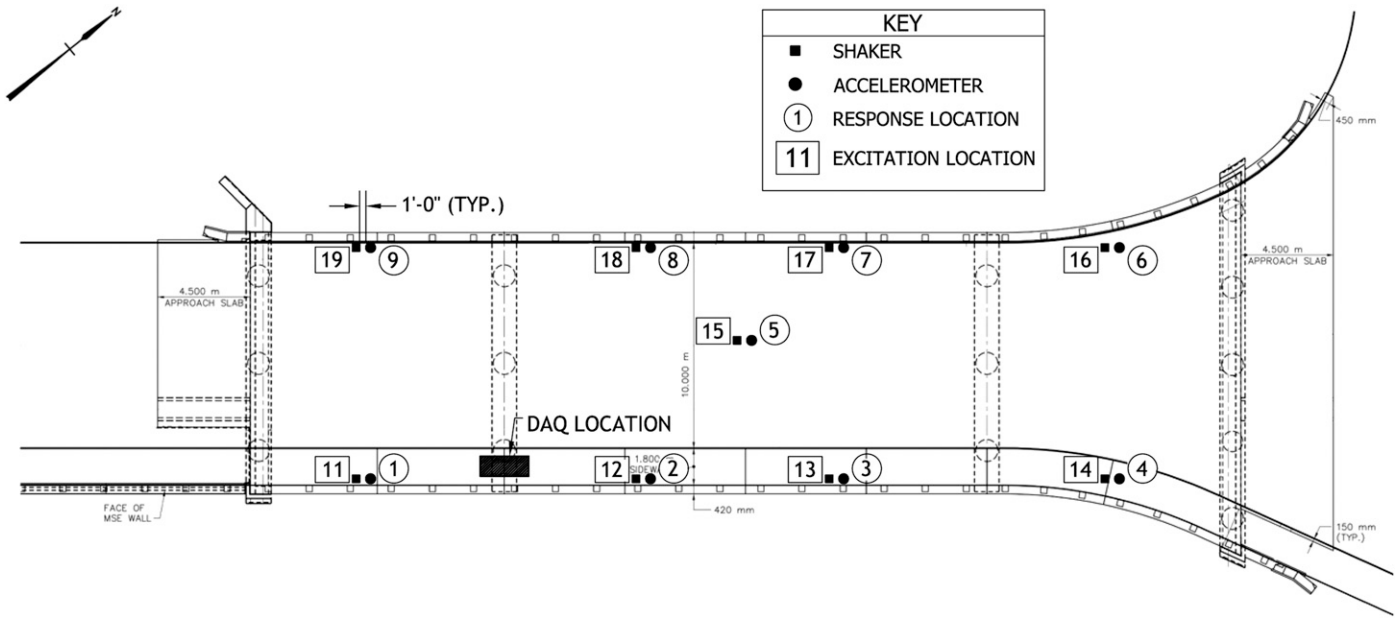

Fig. 3. Shaker and accelerometer layout for dynamic bridge testing

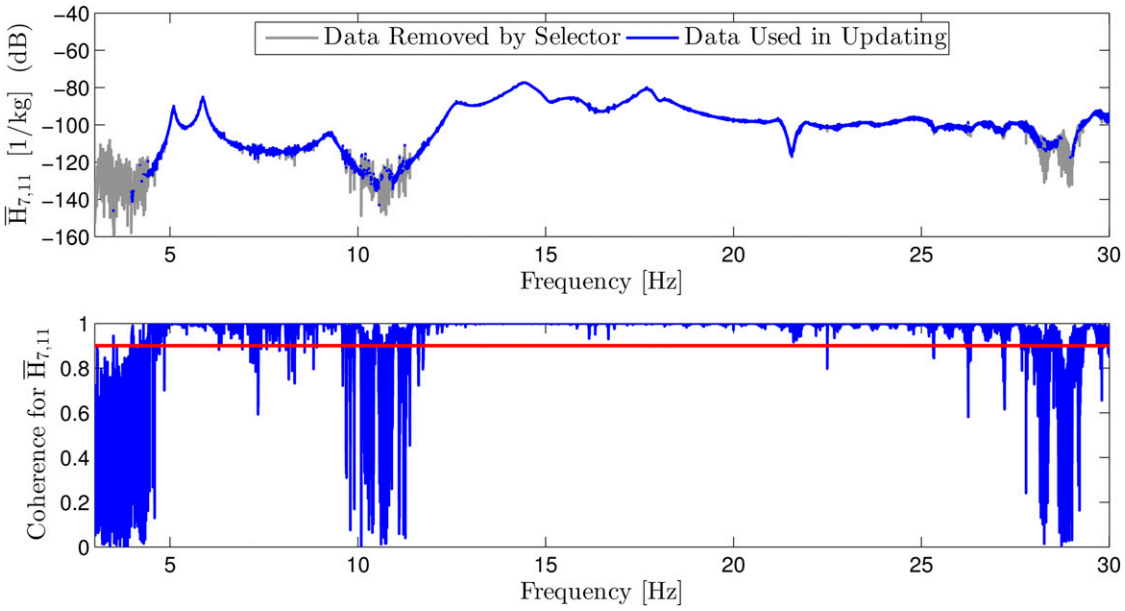

Fig. 4. Sample FRF showing use of coherence selector

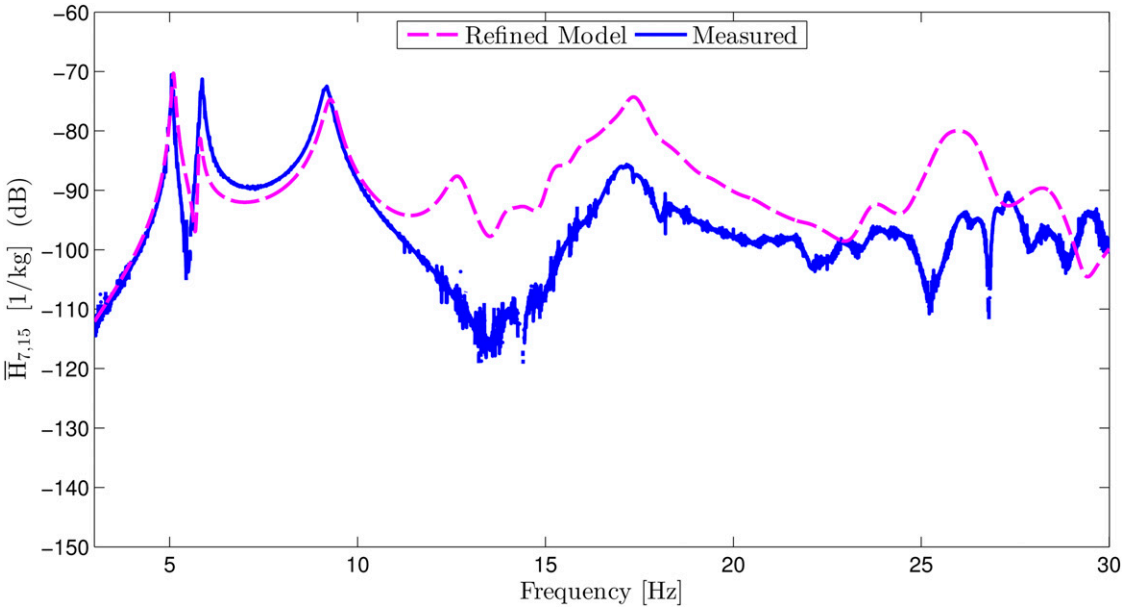

Fig. 5. Sample FRF not used in model calibration

testing. The results from the comparison showed that most of the FRFs had a good match. A pattern started to develop for measurements taken at Location 5 or when the excitation was at Location 15, as shown in Fig. 5. This figure shows the response at Location 7 as a result of excitation at Location 15. Although the first three natural frequencies match, the shape of the FRF does not match well with the FE model after 10 Hz. It was suspected that the positioning of this location at the center of the center span may have been incorrect because it was not close to any features on the bridge, such as the sidewalk or curb. This mismatch and possible error in position were enough to exclude these FRFs from the model calibration, reducing the total number of usable FRFs from 81 to 64.

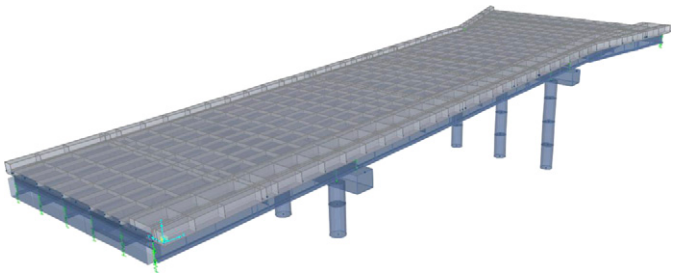

Fig. 6. Graphic representation of PMB FE model

PMB FE Model

This section presents details on how the calibrated model for the PMB was created and verified. Recommendations are provided on how to get a refined FE model that, even without calibration, is a better representation of the structure than a standard FE model such as those used in the design process.

FE Model

The FE model of the PMB, shown in Fig. 6, was created using *CSiBridge 15*. All the geometry was obtained from design drawings provided by the design engineer. Steel members were modeled using an elastic modulus of 200 GPa, a mass density of 7,850 kg/m^3, and as-built cross-sectional properties. The 200-mm-thick concrete deck was modeled using an elastic modulus of 2.60 MPa and a mass density of 2,403 kg/m^3. The element types used were general three-dimensional (3D) beam-column elements for modeling bridge girders and diaphragms, thin shell elements for the bridge deck, and link elements using six degrees of freedom for the boundary conditions. The deck shell elements were offset from the girder frame elements and constrained via nodal coupling to achieve the correct bridge geometry and subsequent behavior. Stiffness values for the linear spring elements were calculated using National Cooperative Highway Research Program (NCHRP) Report 596 (Stanton et al. 2008). The diaphragms and piers were included in the model to keep the model as representative of the 3D structural behavior as possible. This model is referred to as the initial unrefined model. The unrefined model is typically what is used by design engineers to calculate loads and member forces. The model (Fig. 6) shows the geometry extruded. Although not shown for purposes of clarity, nodes are located at the intersections of each frame, shell, and link element.

Because the purpose of this model is to capture dynamic response, careful consideration must be given to accurately modeling both stiffness and mass components of the structure. *CSiBridge* uses lumped-mass modeling; therefore, a model refinement study was performed by subdividing the mesh size until there was no longer a change in model response over the frequency range of interest. This model refinement suggests that the mesh and mass distribution is adequate.

The next step in the modeling process was to include elements that are on the bridge but not normally included in design models. These components include the mass of the stay-in-place forms, the mass of the asphalt wearing surface, the mass of the water pipe supported by the bridge, and the mass of the bridge railings. Using the concrete cylinder samples tested during construction, the stiffness and mass of the concrete curb and sidewalk were modified. The authors had the privilege of being on site during most of the bridge construction, which allowed them a unique perspective. The stiffness and mass of the concrete curb and sidewalk were included even

though a cold joint was present between these elements and the deck because there would be minimal slip at the low tested load levels. The mass of the water pipe, not additional stiffness, was added because techniques were taken to isolate the water pipe from the bridge, including several layers of insulation and wood blocking between the pipe and the structure. Moment releases also were applied to both ends of the diaphragm elements because the physical connection from the diaphragms to the main girders was intended to transfer only shear.

The resulting model is referred to as the refined FE model. The difference between the unrefined and refined models, compared with the measured data, is shown in Fig. 7. Modal damping ratios of 1–2% were used by comparing the analytical FRFs with the measured FRFs. Because modal damping ratios can be easily calculated from experimental data, they are not considered to be unknown parameters in this paper.

The comparison in Fig. 7 shows a drastic improvement in the refined model compared with the measured data. The first three modes of vibration in the refined model correlate well with the measured data. When modeling, initial assumptions can be incorrect, producing an unrefined model that exhibits much different behavior than the actual structure. These gross modeling changes would not necessarily be captured in an automated model calibration because they include the modification of the model geometry. The refined model will be used in the automated calibration.

Analytical FRFs from FE models also can be used as a guide to modelers to determine which components to include in a model based on their influence on the dynamic response of the model. An example of this is the mass of the shear studs or the connection plates that were initially added to the model; however, their addition resulted in no observable change in the analytical FRFs, so they were removed.

Boundary Condition Study

As with all FE modeling, boundary conditions play a major role in the behavior of the model. A study was conducted to determine and verify the stiffness value ranges for the linear spring elements. Simulations were performed by incrementally changing stiffness values and obtaining the resulting response, as shown in Fig. 8. This figure shows the transverse rotational stiffness versus transverse rotation, ranging from 0.0040° at the free condition to 0.00° at the fixed condition. The transverse rotational stiffness, calculated using NCHRP Report 596 (Stanton et al. 2008) and used as the initial parameter value, is shown as a vertical line in Fig. 8. A summary of this study giving the ranges for free, partially restrained, and fixed conditions for the longitudinal, vertical, and transverse rotational stiffness values is presented in Table 1.

FRF-Based FE Model Updating

A method was developed by the authors for FRF-based FE model updating. This method uses commercially available software for both FE modeling and advanced numerical optimization techniques. The fundamental equation of this formulation will be presented in this paper for clarity, whereas the remainder of the formulation can be found in Sipple and Sanayei (2014).

The modal superposition form of the FRF in Eq. (1) is highly efficient for use in parameter estimation because no matrix inversion is required, and only the measured frequency range needs to be considered in the formulation. The form of the FRF in Eq. (1) is accelerance, which is kept consistent throughout this paper, although any form of the FRF can be used in the formulation. The bar over the H in Eq. (1) designates the form used as a variation of the typical form of the FRF as presented in Ewins (2000). This variation uses the magnitude of the FRF in decibel scale for a subset of modes. Thus

$$\overline{H}^{a}_{a,b}(p,\omega) \cong 20 \times \log_{10}\left|\sum_{i=1}^{m}\frac{-\omega^2\hat{\phi}_{ai}(p)\hat{\phi}_{bi}(p)}{-\omega^2+2i\omega\Omega_i(p)\xi_i(p)+\Omega_i^2(p)}\right| \quad (1)$$

where $\overline{H}^{a}_{a,b}$ = analytical form of the FRF at response node a as a result of excitation at node b; i = mode shape and associated natural frequency ranging from 1 to m, which is a subset of the total kinematic degrees of freedom n; $\hat{\phi}_{ai}$ and $\hat{\phi}_{bi}$ = scalar values of mode shape i at response node a and excitation node b; Ω_i = natural frequency scalar value for mode i; ξ_i = modal damping ratio for

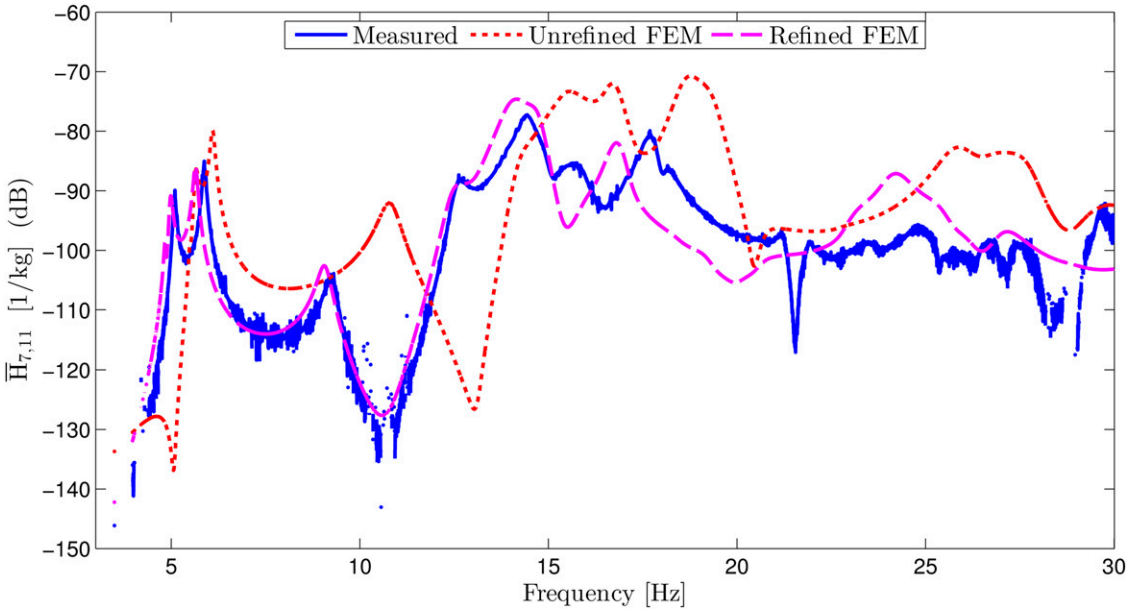

Fig. 7. Measured FRF compared with unrefined and refined FE models

J. Bridge Eng.

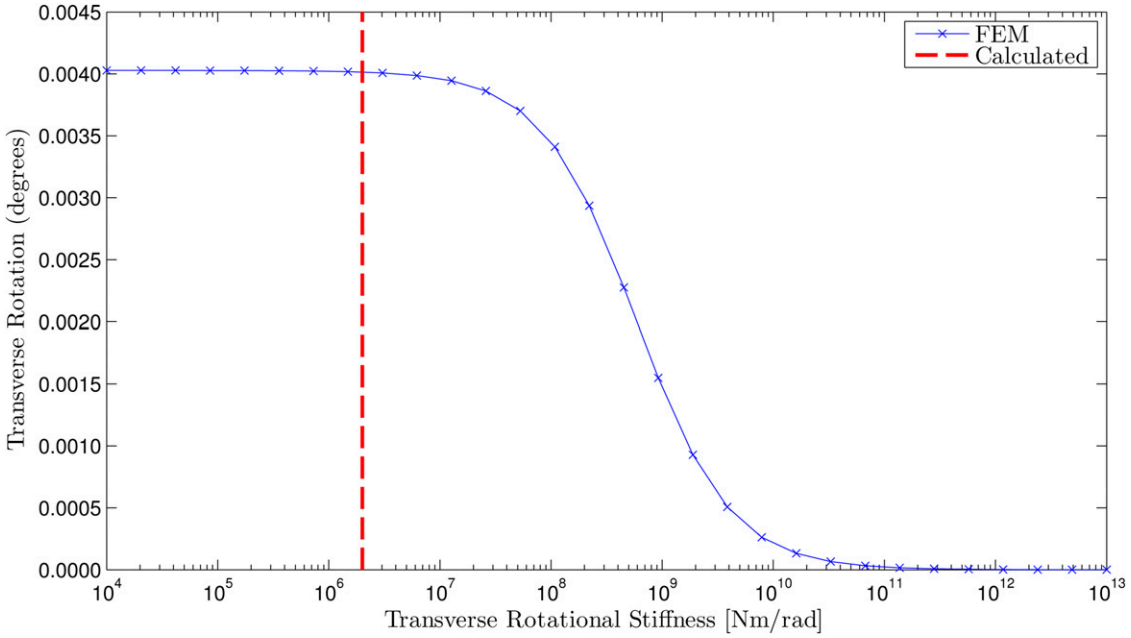

Fig. 8. Sample FE model analysis to determine boundary stiffness ranges

Table 1. Linear Spring Stiffness Values for Elastomeric Bearing Pads

	Boundary stiffness ranges			
Stiffness direction	Free	Partially restrained	Fixed	Calculated
Longitudinal (N/m)	$<8\times10^3$	8×10^3 to 4×10^{10}	$>4\times10^{10}$	1.117×10^6
Vertical (N/m)	—	Up to 2×10^{10}	$>2\times10^{10}$	6.313×10^8
Transverse rotation (N · m/rad)	$<6\times10^6$	6×10^6 to 1×10^{11}	$>1\times10^{11}$	2.007×10^6

mode i; p = structural parameter that is being updated; and ω = frequency range of interest. The form of Eq. (1) allows for simultaneous estimation of stiffness, mass, and damping parameter.

The parameters p are unitless modifiers that adjust the structural parameters of the FE model. The values of p typically have a range from 0.1 to 2, with an unchanged parameter having a value of 1. These parameter bounds were chosen to keep the properties within a reasonable range while allowing the constrained optimization to freely estimate the parameters. Global search techniques are also used to explore the bounded region and give additional confidence, through repeatability of estimated parameters and engineering judgment, that the estimated parameters can be at the global minimum. Examples of the structural parameters to be modified are axial rigidity and strong-axis bending rigidity of individual elements or elements in a group. The term rigidity refers to the EA term for axial rigidity or the EI term for bending rigidity as opposed to just modifying the modulus of elasticity E or geometric properties (A = area and I = moment of inertia) separately. These parameters are used to modify any structural element type available in the FE model.

To perform the optimization, several different techniques were used, including development of a FRF-based error function, creation of a scalar objective error function, and subsequent minimization of that objective function. The FRF-based error function is simply the difference between the analytical and measured FRFs. The scalar objective function is a least-squares error function that allows the value J to be minimized through constrained optimization.

Observability and Identifiability of Structural Parameters

Prior to model calibration, a sensitivity study was performed to determine which structural parameters caused a change in the analytical FRFs and therefore could be considered to be observable. Stiffness and mass parameter updating will be the focus of this study because a change in either stiffness or mass causes a shift in the FRF along the frequency axes. Modifying the damping values will only control the sharpness of the FRF peaks at the natural frequencies. To perform this study, a parameter modifier of 0.80 was applied to each structural property modifier, and this modified FRF was compared with the initial FRF. To quantify the difference caused by a 20% reduction, the norm of the FRF-based error-function vector was used as a comparative guide to determine which parameters were observable. The observable parameters were found to be girder axial rigidity, girder strong-axis bending rigidity, deck rigidity, deck mass, and boundary stiffness in the longitudinal, vertical, and transverse rotation directions. The larger groups, such as deck rigidity and deck mass, can be subdivided because of their large observability. Parameters that were not observable were girder shear rigidity, girder torsional rigidity, and girder weak-axis bending rigidity.

Simulations must be performed to ensure that these parameters are identifiable in simultaneous parameter estimation. The two main reasons that parameters may be individually observable but not identifiable are linear dependencies and ill-conditioning. Through these simulations, it was determined that, for example, deck mass and deck rigidity are not identifiable when used at the same time. The parameters chosen in the model calibration must be both observable and identifiable for the model calibration to be viewed as a success.

Selection of Unknown Parameters

Five unknown parameter groups were selected. The three parameter groups chosen for calibration of the bridge superstructure were deck rigidity for positive bending, negative bending, and sidewalk and curb regions. The negative bending regions are the areas adjacent to

the piers that transition to positive bending regions in the remaining portion of each of the three spans. Each negative bending region covers the length of the negative bending steel reinforcement that was included in the final design of the bridge. Vertical and transverse rotational stiffness values of all bearing pads are the two remaining parameter groups. All initial parameter values used for the simulation and subsequent calibration are shown in Table 2. The values shown for the concrete regions are an equivalent stiffness, shown here as an equivalent modulus of elasticity E. The geometric properties were kept constant and are based on the as-built bridge. Further ungrouping of these parameters was attempted, but because of issues with identifiability of parameters, it was concluded that this was the best combination of parameters to use in FE model calibration.

Table 2. Initial Parameter Values for Simulations and Model Calibration

Parameter	Value
Positive bending region (GPa)	27.2
Negative bending region (GPa)	27.2
Sidewalk curb (GPa)	27.2
Transverse rotation stiffness (N · m/rad)	2.01×10^6
Vertical stiffness (N/m)	6.31×10^8

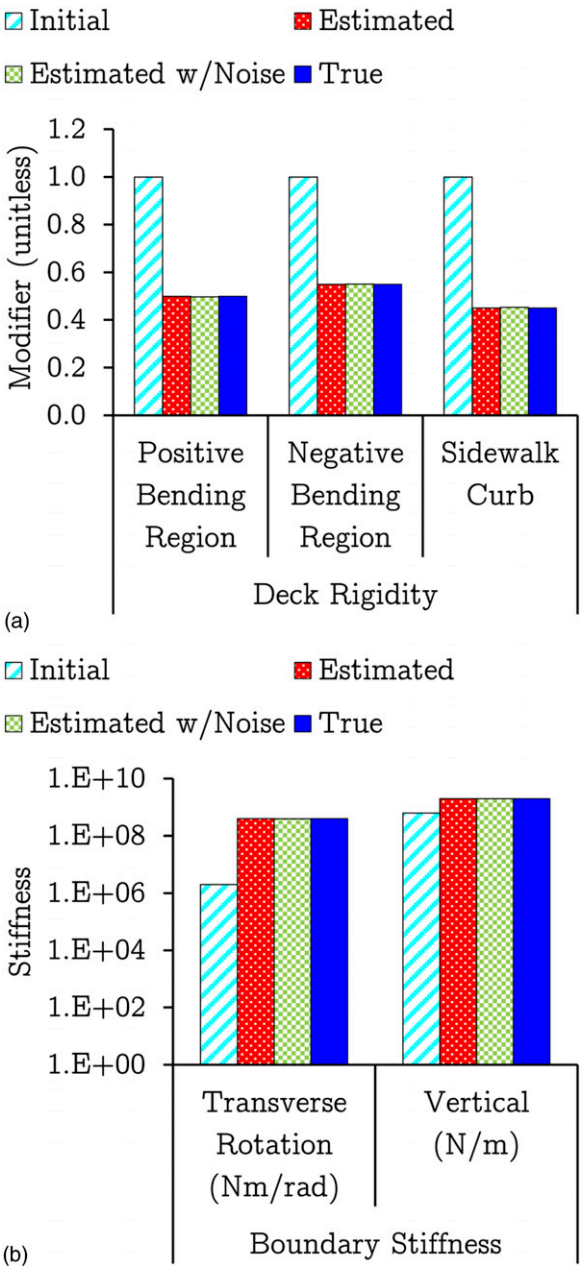

Fig. 9. Simulation results showing (a) deck rigidity parameter modifiers; (b) boundary stiffness values

Simulated FE Model Calibration to Ensure Identifiability

To verify that the selected parameters for calibration are identifiable, simulations were performed with that same group of unknown parameters. The simulations were performed both with and without measurement noise. The measurement noise used in the simulations was the ambient vibration data from the 2011 bridge test, providing measurement noise that was as real as possible. The simulated true values were selected to show that the method is able to capture large changes in parameters.

Fig. 9 shows a perfect match between the estimated and true parameters from simulations using automated FRF-based FE model updating. The difference between estimated parameters with noise and true parameters was less than 1%, showing the accuracy of the estimates in the presence of measurement error. Although the results are shown in two separate graphs, the parameter estimation was performed simultaneously. Fig. 9(a) shows parameter modifier values for deck rigidity, and Fig. 9(b) shows the boundary stiffness values. The values shown in Fig. 9 are also listed for clarity in Table 3.

The FRF in Fig. 10 shows what is also seen in Fig. 9: the parameter estimation correctly identified all the parameters to be included in the calibration both with and without measurement noise. This successful simulation provides confidence that the calibration using measured data can estimate realistic changes in the unknown parameters when moving the analytical FRF to the measured FRF. The sample FRF, $\overline{H}_{7,11}$, is an accurate representation of the quality of improvement in all the other FRFs used in these simulations and future calibration results.

Discussion of Unknown Parameters

At this point in the discussion, it is worth clarifying, in addition to the results from the identifiability and observability study, the unknown parameters that were used in the simulations and will be used for model calibration. The deck rigidity parameter refers to an equivalent stiffness of the concrete deck. Although changing the deck rigidity has an effect on the behavior of the structure, a change in deck rigidity only partially contributes to a change in the bridge cross section because of its location off the neutral axis. Beam rigidity and beam stiffness were not used as unknown parameters because the properties of steel beams are generally known and accepted as true. Although the deck rigidity and mass cannot be identified simultaneously and may be viewed as a challenge, there is high confidence because of construction control in the final thickness of the concrete deck and subsequent mass. The parameters contributing to unknown structural behavior of the bridge align with the parameters chosen for identification and include bending rigidity of the concrete deck and stiffness of the boundary conditions.

FE Model Calibration of the PMB Using Measured FRFs

The calibration using measured FRFs was performed with the same five parameter groups as used in the simulations. The results of the

Table 3. Simulation Results for Deck Rigidity Parameter Modifiers and Boundary Stiffness

Parameter type	Parameter	Initial	Estimated	Estimated with noise	True
Deck rigidity (parameter modifiers)	Positive bending region	1.000	0.500	0.498	0.500
	Negative bending region	1.000	0.550	0.551	0.550
	Sidewalk curb	1.000	0.450	0.453	0.450
Boundary stiffness (values)	Transverse rotation (N · m/rad)	2.007×10^6	4.000×10^8	3.995×10^8	4.000×10^8
	Vertical (N/m)	6.313×10^8	2.000×10^9	1.984×10^9	2.000×10^9

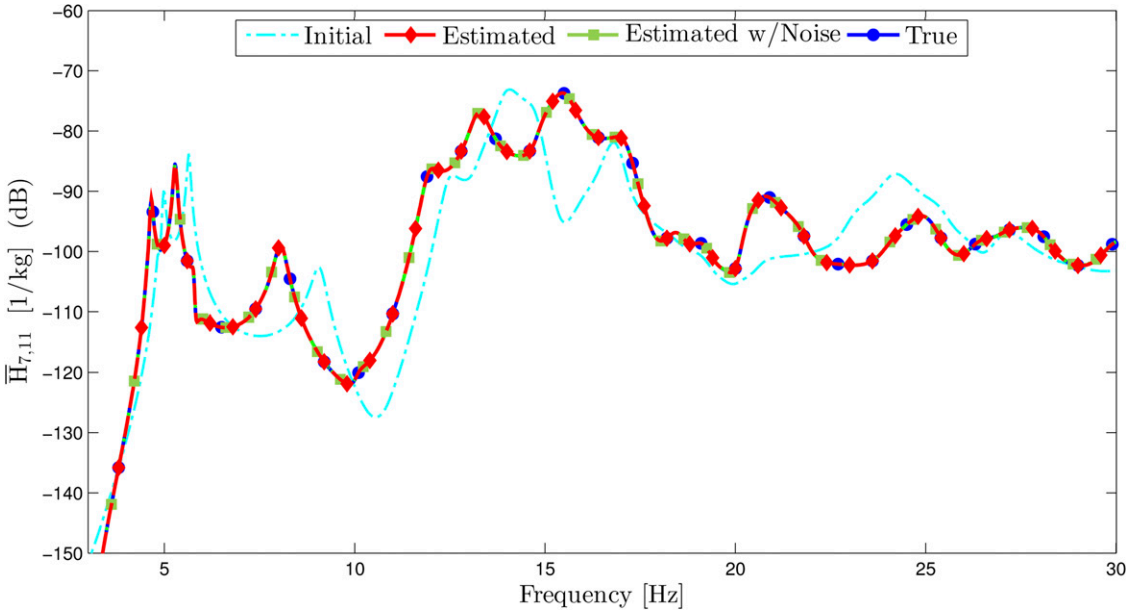

Fig. 10. Sample FRF for successful simulated identification

calibration are shown in Figs. 11 and 12. Fig. 11 shows initial and estimated parameter values using all 64 FRFs and a subset of 49 FRFs. A subset of FRFs was used to ensure that the identified parameters did not depend on the number of FRFs used. Fig. 12 shows the refined-model FRF, which corresponds to the initial parameters; the calibrated-model FRF using all FRFs, which corresponds to the estimated parameters using all FRFs; the calibrated-model FRF using a subset of FRFs, which corresponds to the estimated parameters using a subset of FRFs; and the FRF measured from the 2011 bridge test. The FRFs in Fig. 12 are for the measured response at Node 7 as a result of excitation at Node 11. The values shown in Fig. 11 are also listed for clarity in Table 4.

Examining the results in Fig. 11, Fig. 11(a) shows the shell rigidity modifier estimates for bridge deck stiffness, whereas Fig. 11(b) shows the boundary stiffness values for the bearing pads. Although the results are displayed in two separate graphs, these five unknown parameter groups were estimated simultaneously. The most interesting result, and largest change from the initial values, was the negative bending region shell rigidity with an increase of 56%. This result was investigated by examining the design drawings, where it was observed that two times the amount of steel reinforcement was placed in the top layer of rebar in this area. The additional reinforcement was not included in the refined FE model because the deck was modeled as plain concrete. A hand calculation using full composite action between the RC deck and steel girders was performed and verified the 56% increase in negative bending region deck rigidity. For this calculation, the shell elements were modeled using an equivalent stiffness that takes into account the presence of the steel reinforcement. Further analysis of the results showed no significant change, nothing greater than 4%, in any of the other parameters. These small changes can be the result of the influence of modeling and measurement errors. Although the changes in spring stiffness appear to be large, neither parameter moved outside its initial characterization. To quantify the improvement of the different FE models, the second norm of the error function was calculated between the measured data and the different models. Moving from the unrefined to the calibrated model showed 44% improvement. This ratio will never reach the ideal value of 100% because of the presence of measurement and modeling errors.

The difference between the parameter estimates of the calibrated models using all FRFs and a subset of FRFs was no more than 4%. This small change is considered to be within the acceptable range of parameter estimates in the presence of modeling and measurement errors. A slight change in the transverse rotational stiffness values also was observed, but the estimated value was still within the range for free rotation. The similarity between the results using all and a subset of FRFs shows that the method can accurately estimate unknown parameters with a smaller group of measurements.

The FRFs in Fig. 12 show that there is improvement from the refined model to the calibrated model. In the lower frequency range, there is an excellent match between the calibrated FE model and the measured FRF for the first five modes. The shape of the FRF for the calibrated model follows the shape of the measured FRF after 15 Hz but deteriorates as the frequency gets higher. Although the match is not perfect, the authors feel that it is important to display the full measured frequency range. This reduced match could be caused by

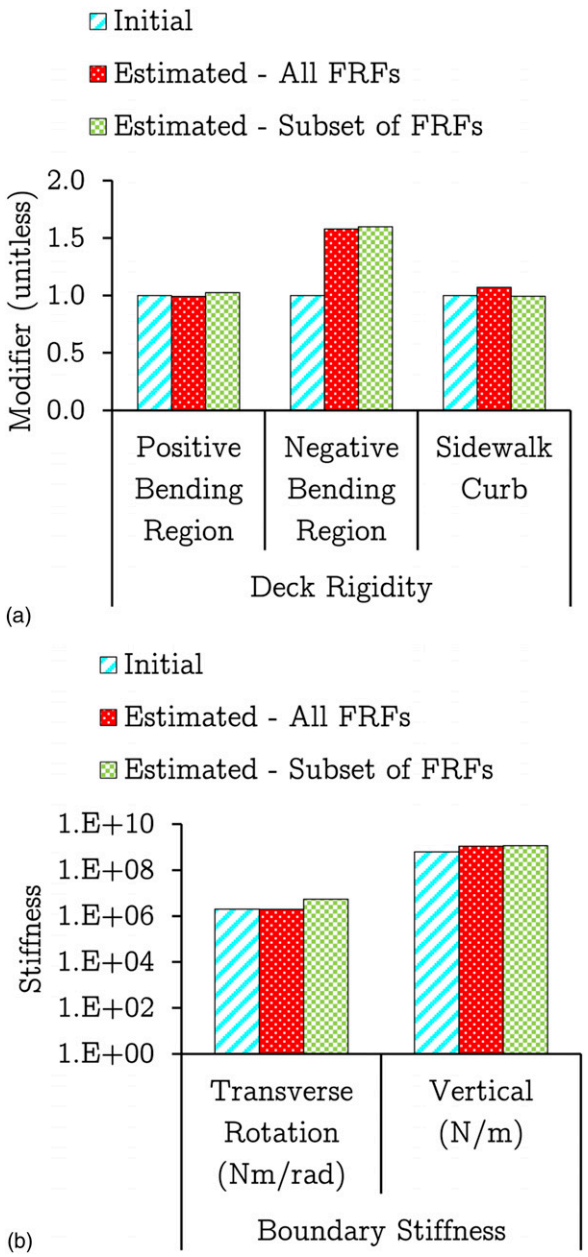

Fig. 11. Model calibration results using measured FRFs showing (a) shell rigidity parameter modifiers; (b) boundary stiffness values

the inability of the FE model to capture the behavior in that frequency range. The behavior in this range is more affected by local effects, whereas the global behavior of the structure is observed in the lower frequency range.

Verification of Results

The FRFs not included in the subset are viewed as a control group. Response and excitation at Nodes 8 and 18 were randomly removed from the original set of 64 FRFs, resulting in the subset of 49 FRFs. The FRF from the control group is shown in Fig. 13 and is for the measured response at Node 3 as a result of excitation at Node 18. Comparing the refined, calibrated, and measured FRFs in Fig. 13, the calibrated model matches well with measured data up to 15 Hz for five modes and following similar trends to those seen in Fig. 12.

An additional verification was done by calibrating the same model using measured FRFs from the 2010 bridge test. The estimated parameters from this calibration were no more than 5% different from the estimated parameters from the calibration using the 2011 bridge data. This difference is again considered to be within the acceptable range of parameter estimates using data from two different years and for different environmental conditions.

Summary of Results

The process of model calibration is extensive and requires careful planning. A FE model was created initially using design information to define both geometric and structural parameters of the model. This unrefined FE model then was manually adjusted to include specific elements not typically included in a design model, as-built information, and components that influence the dynamic response of the bridge. These additional elements included diaphragms, sidewalks, curbs, and additional mass elements, resulting in the refined FE model. A sensitivity analysis then was performed to find the identifiable and observable parameters for use in calibration. Simulations also were performed with the presence of measurement error to ensure that the selected parameters were estimated accurately. These parameters then were used to automatically update the FE model using the measured test data, resulting in a calibrated FE model. The estimated parameters were compared with the engineering drawings for validity using engineering calculations and judgment. Additional verifications were performed to check the results using only a subset of measured data as well as data from a previous year's test.

This research demonstrates that calibration of a full-scale bridge is feasible using the FRF-based FE model updating method. The unknown structural parameters that are individually observable also must be identifiable when combined with other observable parameters. This is accomplished by performing simulations in the presence of measurement error with the parameters to be used in the calibration.

The calibration results provide an acceptable match at lower frequencies. In the higher frequency range, the match improved but was not perfect. This mismatch at higher frequencies is expected when trying to model a full-scale structure with an idealized FE model. Local effects influence the measured FRFs much more in the higher frequency range, whereas the FE model is intended to simulate global behavior. Further subdividing of the parameter groups was done to improve the match at higher frequencies, but calibration was not possible because these smaller groups were neither observable nor identifiable when tested in simulations. The FRFs shown for both the calibration and simulations represent a typical match between FRFs.

The calibration provides adjustments that were originally overlooked by the authors when creating the refined FE model. The calibration using FRFs was performed in an efficient manner; computation time required for convergence with one set of initial parameter values was approximately 30 min on a personal computer with an average of 20 iterations.

Verification of the calibration confirmed the validity of the estimated parameters when comparing the calibrated model with the measured test data that were not used in FE model calibration. The results also were verified when performing calibration using the 2010 measured data and resulted in similar estimated parameters.

The biggest change in the analytical FRF was seen between the unrefined and the refined FE models. Use of the refined FE model

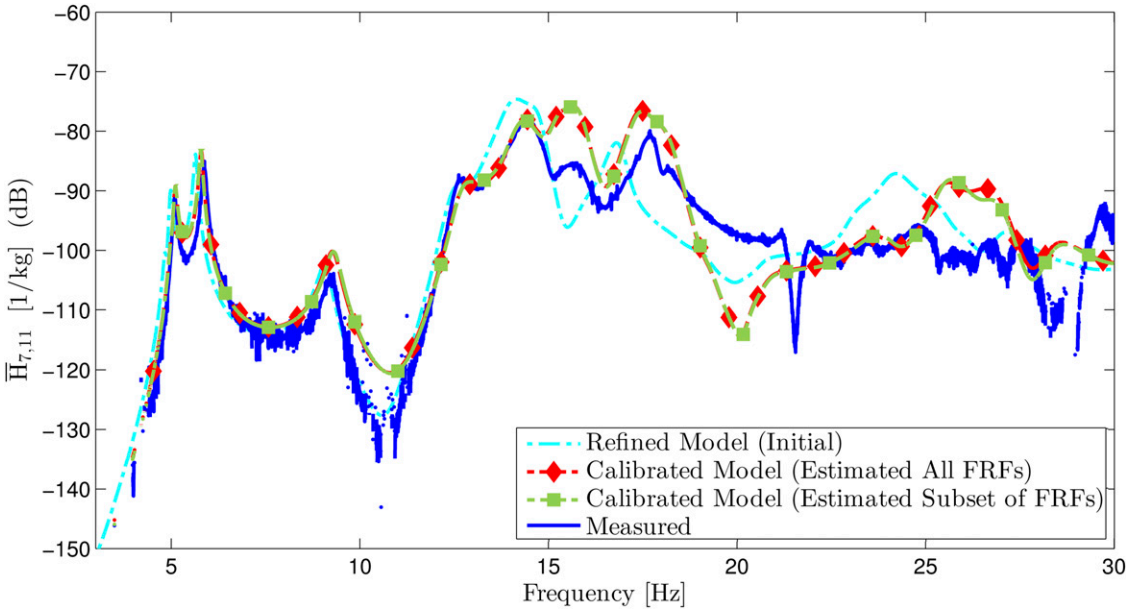

Fig. 12. FE model calibration sample FRF

Table 4. Model Calibration Parameters for Deck Rigidity and Boundary Stiffness

Parameter type	Parameter	Initial	Estimated, all FRFs	Estimated, subset of FRFs
Deck rigidity (parameter modifiers)	Positive bending region	1.000	0.995	1.026
	Negative bending region	1.000	1.562	1.600
	Sidewalk curb	1.000	1.036	0.994
Boundary stiffness (values)	Transverse rotation (N · m/rad)	2.007×10^6	3.526×10^6	5.455×10^6
	Vertical (N/m)	6.313×10^8	1.148×10^9	1.158×10^9

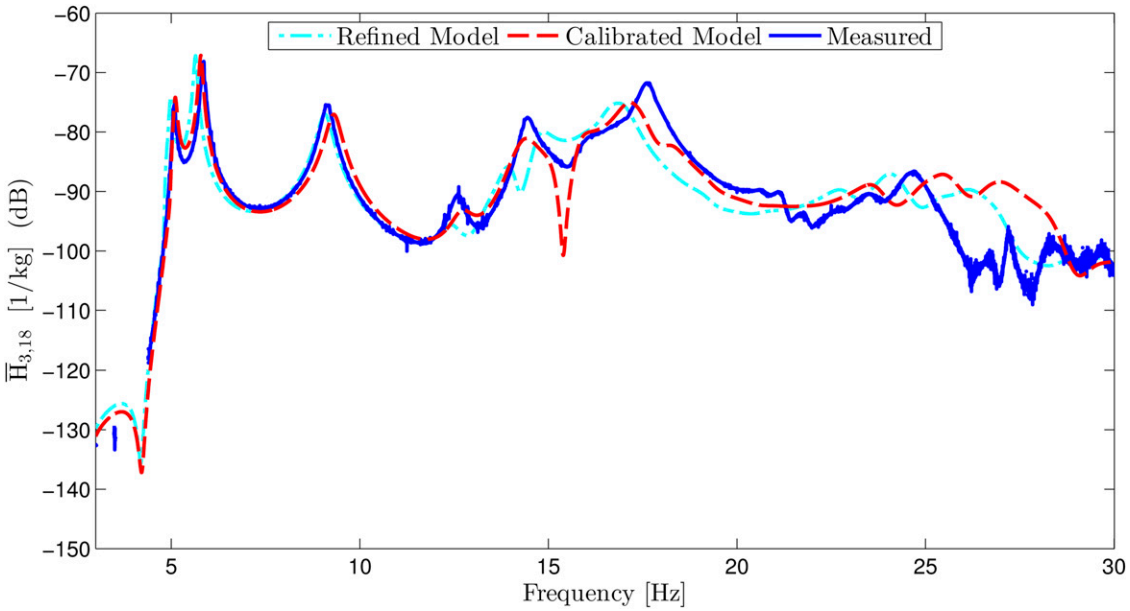

Fig. 13. Sample FRF from control group

led to a very good match for the first three modes of vibration, and the automated calibration allowed for a closer match.

Future work would include determining whether this calibrated model is capable of capturing live-load girder distribution factors, which is an essential tool for practicing engineers in developing accurate load ratings. Using static test data and a model calibrated by this method would provide insight into how a dynamically calibrated model can predict static behavior and therefore load

distribution. These additional studies will be able to determine whether the lateral stiffness is both accurately modeled and excited using the techniques from this paper.

Conclusions

A FRF-based FE model updating method was applied to a full-scale bridge while investigating dynamic testing methods and the ability to identify parameters. An unrefined FE model was created initially based on construction documents and was updated to include elements not typically seen in a design FE model. Visual improvements were seen when comparing the refined FE model with the measured FRFs. This comparison also showed how FRFs can be used as a guide for engineers when creating FE models of existing structures. Challenges dealing with ill-conditioning and linear dependency were observed in the simulations. The simulated FRF-based FE model updating was used not only to show that the method can be used with full-scale structures but also to aid in model creation, where parameters were chosen to be identified during model calibration. The results from the simulations showed less than 1% difference between the estimated parameters and the expected true values both with and without measurement noise.

Model calibration was performed successfully, showing improvement over the refined FE model. The deck rigidity for shell elements in the negative bending region increased by 56% during model calibration. This increase corresponded to an increase in steel reinforcement that was not included in the original model. All the other parameters had a change of less than 4%. Examining the second norm of the residual between the different models and the measured data resulted in a 44% improvement from the unrefined to the calibrated FE model. Verifications also were performed using a subset of measured data as well as data from the 2010 test, and both showed less than 5% change in parameters.

Creating the refined model and performing automated calibration resulted in a model that was a better representation of the bridge than simply creating a model based on construction drawings. The calibrated FE model could be used as an objective tool for long-term bridge management that would provide bridge owners with the ability to quantitatively track the structural performance of their bridges through modeling and periodic testing. Some of the additional uses for the calibrated FE model are response-prediction applications, which could include bridge widening, permit loading, construction staging, structural repairs, and service planning.

Acknowledgments

The authors are grateful for the funding of this research made possible by National Science Foundation PFI Grant 0650258. Any opinions, findings, and conclusions or recommendations expressed in this paper are those of the authors and do not necessarily reflect the views of the National Science Foundation.

References

Bell, E. S., Lefebvre, P. J., Sanayei, M., Brenner, B., Sipple, J. D., and Peddle, J. (2013). "Objective load rating of a steel-girder bridge using structural modeling and health monitoring." *J. Struct. Eng.*, 10.1061/(ASCE)ST.1943-541X.0000599, 1771–1779.

Catbas, F. N., Kijewski-Correa, T., and Aktan, A. E., eds. (2013). *Structural identification of constructed systems: Approaches, methods, and technologies for effective practice of St-Id*, ASCE Structural Engineering Institute, Reston, VA.

CSiBridge 15 [Computer software]. Berkeley, CA, Computers and Structures.

Ettouney, M. M., and Alampalli, S. (2011). *Infrastructure health in civil engineering*, CRC Press, London.

Ewins, D. (2000). *Modal testing: Theory, practice and application*, 2nd Ed., Research-Studies Press, Letchworth, U.K.

Farrar, C. R., and Jauregui, D. A. (1998). "Comparative study of damage identification algorithms applied to a bridge: I. Experiment." *Smart Mater. Struct.*, 7(5), 704–719.

Farrar, C. R., and Worden, K. (2007). "An introduction to structural health monitoring." *Philos. Trans. R. Soc. London, Ser. A*, 365(1851), 303–315.

Karbhari, V. M., and Ansari, F., eds. (2009). *Structural health monitoring of civil infrastructure systems*, Woodhead Publishing, Oxford, U.K.

Mottershead, J. E., and Friswell, M. I. (1993). "Model updating in structural dynamics: A survey." *J. Sound Vib.*, 167(2), 347–375.

Pavic, A., Armitage, T., Reynolds, P., and Wright, J. (2002). "Methodology for modal testing of the Millennium Bridge, London." *Proc. Inst. Civ. Eng. Struct. Build.*, 152(2), 111–121.

Sanayei, M., Phelps, J. E., Sipple, J. D., Bell, E. S., and Brenner, B. R. (2012). "Instrumentation, nondestructive testing, and finite-element model updating for bridge evaluation using strain measurements." *J. Bridge Eng.*, 10.1061/(ASCE)BE.1943-5592.0000228, 130–138.

Sipple, J. D. (2014). "Frequency response based finite element model updating." Ph.D. thesis, Tufts Univ., Medford, MA.

Sipple, J. D., and Sanayei, M. (2014). "Finite element model updating using frequency response functions and numerical sensitivities." *Struct. Control Health Monit.*, 21(5), 784–802.

Sohn, H., Farrar, C. R., Hemez, F., and Czarnecki, J. (2004). *A review of structural health monitoring literature: 1996–2001*, Los Alamos National Laboratory, Los Alamos, NM.

Stanton, J. F., Roeder, C. W., Mackenzie-Helnwein, P., White, C., Kuester, C., and Craig, B. (2008). "Rotational limits for elastomeric bearings." *NCHRP Rep. 596*, Transportation Research Board, Washington, DC.

Živanović, S., Pavic, A., and Reynolds, P. (2007). "Finite element modelling and updating of a lively footbridge: The complete process." *J. Sound Vib.*, 301(1–2), 126–145.